

Realization of charge-four Weyl point in fermionic systems

Xiaoliang Xiao ¹, Yuanjun Jin ², Da-Shuai Ma,^{1,3} Weixiang Kong,¹ Jing Fan,⁴ Rui Wang ^{1,3,5} and Xiaozhi Wu^{1,5,*}

¹*Institute for Structure and Function & Department of Physics, Chongqing University, Chongqing 400044, People's Republic of China*

²*Division of Physics and Applied Physics, School of Physical and Mathematical Sciences, Nanyang Technological University, Singapore 637371, Singapore*

³*Center of Quantum materials and devices, Chongqing University, Chongqing 400044, People's Republic of China*

⁴*Center for Computational Science and Engineering, Southern University of Science and Technology, Shenzhen 518055, People's Republic of China*

⁵*Chongqing Key Laboratory for Strongly Coupled Physics, Chongqing 401331, People's Republic of China*



(Received 6 April 2023; revised 4 July 2023; accepted 28 July 2023; published 14 August 2023)

Unconventional quasiparticles of a twofold band degeneracy with $|C| = 4$, named as charge-four Weyl point (CFWP), have been revealed in bosonic and artificial systems, while it is challenging in fermionic systems because of nonnegligible spin-orbit coupling. Herein, we propose a carbon allotrope, termed cP-C24, as an ideal platform to realize CFWP in the nonrelativistic limit. Besides one CFWP ($C = +4$), there are also eight type-I Weyl points ($C = +1$) and twelve type-II Weyl nodes ($C = -1$), making the topological charge in the whole Brillouin zone to be neutral. The characteristic quadruple helicoid surface states of CFWP are presented. Our work offering the avenue of CFWP in fermionic systems would absolutely advance the research on the chirality-dependent physical properties associated with unconventional topological quasiparticles.

DOI: [10.1103/PhysRevB.108.075130](https://doi.org/10.1103/PhysRevB.108.075130)

I. INTRODUCTION

The crystallographic space group (SG) symmetry in condensed matter physics is much lower than the Poincaré symmetry in high energy physics [1,2]. Consequently, unconventional quasiparticles without high-energy counterparts have been proposed in the past decade [1–4]. Systems with conventional quasiparticles, such as Dirac and Weyl fermions, are experimentally reported to possess novel physical properties, e.g., chiral zero sound [5,6] and negative magnetoresistance caused by chiral anomaly [7–12]. Distinct from Dirac and Weyl fermions, unconventional quasiparticles with larger topological charge [1–4,13–17] are particularly attractive because they have unique physical properties, such as larger quantized circular photogalvanic effect (CPGE) [18–20], longer Fermi arc surface states [21–27], quantum criticality and phase transition [28,29], non-Fermi-liquid interaction effects [30,31], etc. With the consideration of crystallographic SG symmetry, the largest topological charge for a twofold degenerated point is proven up to $|C| = 4$ in spinless systems [32–36]. Thus, this kind of twofold charge-four Weyl point (CFWP) is mainly realized in bosonic and artificial systems [32,33,37–39], while there is still a lack of natural material to achieve CFWP in fermionic systems.

The main obstacle here is that the spin-orbit coupling (SOC) is usually nonnegligible in fermionic systems. Thus, described by the double-valued representation of SG, the charge-four twofold degenerate point is not allowed in electronic systems [32,35]. Fortunately, compounds composed of

light atoms are viewed as an ideal platform for achieving topological states permitted in systems with SU(2) spin-rotational symmetry [40]. Over the past decade, various topological states, such as nodal points, nodal lines, and nodal surfaces, have been revealed in light-atom-composed compound, e.g., boron and carbon allotropes both theoretically and experimentally [41–54]. Especially carbon, the most abundant and versatile element with negligible SOC [55], possesses a rich variety of allotropes [56]. The carbon allotropes are reported to have various crystalline symmetries [57,58], which leaves the carbon allotropes being ideal candidates to reveal symmetry-protected unconventional quasiparticles. Therefore, it is feasible to search for a class of carbon allotropes with the relevant SGs that allow the existence of CFWPs.

Here, based on the symmetry arguments and first-principles calculations, we identify a carbon allotrope, namely cP-C24, as an ideal material candidate to host CFWP in the nonrelativistic limit. This carbon allotrope is crystallized in SG P4₁32 (No. 213) with an sp² hybridized network. The analysis shows that one CFWP with $C = +4$ emerges at the center of the Brillouin zone (BZ) protected by cubic symmetry. Additionally, there are also eight type-I Weyl points (WPs) with $C = +1$ along four diagonals and twelve type-II Weyl nodes with $C = -1$ in the BZ, leading to the neutral topological charge. Due to the bulk-boundary correspondence, the topological charge of +4 results in the quadruple helicoid surface states, linking one CFWP and four type-II WPs, which is considered as evidence of CFWP. The results show the carbon allotrope cP-C24 is a promising platform for exploring various topological fermions, including CFWP, type-II Weyl, and conventional Weyl fermions.

*xiaozhiwu@cqu.edu.cn

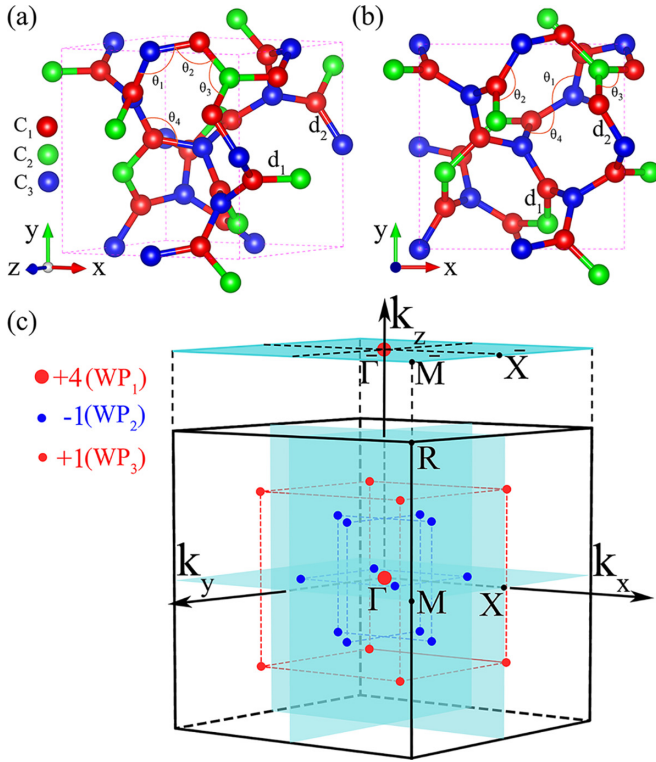


FIG. 1. (a) Side and (b) top views of cP-C24 with an sp^2 hybridized network. The carbon atoms occupy three types of Wyckoff positions: 12d(0.125, 0.205, 0.455), 4b(0.875, 0.875, 0.875), and 8c(0.501, 0.501, 0.501), denoted by C₁ (red balls), C₂ (green balls), and C₃ (blue balls), respectively. (c) The bulk BZ and the projected (001) surface BZ, respectively. The marked dots in red (big and small) and blue (small) in the BZ are the WPs characterized by the topological charges of +4, +1, and -1, respectively.

II. THE STRUCTURE, STABILITY, AND ELECTRONIC PROPERTIES

First, we employ the first-principles calculations based on the density functional theory [65,66] [see the computational method in the Supplemental Material (SM) [67]] to elucidate electronic properties of cP-C24. As illustrated in Figs. 1(a) and 1(b), cP-C24 possesses 24 carbon atoms in the cubic unit cell with SG $P4_32$ (No. 213). Its optimized lattice parameter is estimated to be $|\mathbf{a}| = 5.96$ Å. The carbon atoms occupy three types of Wyckoff positions: 12d (0.125, 0.205, 0.455), 4b (0.875, 0.875, 0.875), and 8c (0.501, 0.501, 0.501), denoted by C₁ (red balls), C₂ (green balls), and C₃ (blue balls), respectively. These agree well with previous publication [64]. One can find that each C₁ atom is bonded to one C₂ and two C₃ atoms, while each C₂ (or C₃) atom is only connected to three C₁ atoms. Thus, it reveals that cP-C24 is an sp^2 hybridized network. In contrast to the unique sp^2 bond lengths in graphite (1.42 Å), there are two distinct carbon-carbon bond lengths, i.e., $d_1 = 1.43$ Å for C₁-C₂, and $d_2 = 1.46$ Å for C₁-C₃. In addition, compared with the sp^2 bond angles in graphite (120°), there are four different bond angles, i.e., $\theta_1 = 120^\circ$ for C₁-C₃-C₁, $\theta_2 = 117.8^\circ$ for C₃-C₁-C₂, $\theta_3 = 119.2^\circ$ for C₁-C₂-C₁, and $\theta_4 = 124.4^\circ$ for C₃-C₁-C₃.

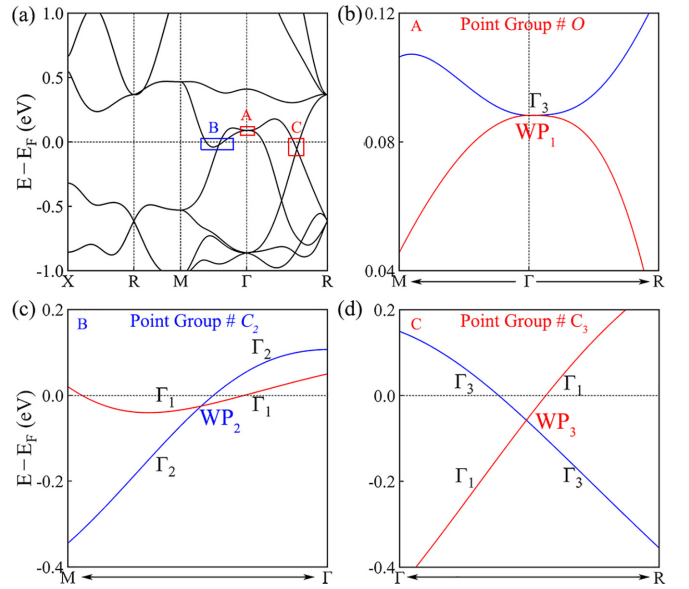


FIG. 2. (a) The bulk electronic band structure of cP-C24 along high-symmetry paths. The crossings of two bands near the Fermi level are marked quadrangles of A, B, and C. (b)–(d) The enlarged drawings of energy dispersion around WPs, i.e., WP₁ (CFWP), WP₂ (type-II WP), and WP₃ (type-I WP). The relevant IRs are marked with the corresponding PGs O , C_2 , and C_3 , respectively.

To investigate the stability of cP-C24, the calculated total energies as functions of volume per atom for different carbon allotropes are plotted in Fig. S1 in the SM [67]. The volume-dependent total energies of Diamond, T carbon, and cP-C24 keep the great agreement with that given in Ref. 64 [64]. For comparing with reported data [48,59–63], the calculated lattice parameters, total energies per atom E_{tot} , and energy gaps E_g are also listed in Table I. The E_{tot} for cP-C24 is -8.453 eV/atom, which is 0.534 eV/atom lower than T carbon. Since T-carbon nanowires were successfully synthesized [53], it is anticipated that cP-C24 can also be synthesized experimentally under favorable conditions. Furthermore, the phonon dispersion calculation and density-functional-based *ab initio* molecular dynamics (AIMD) simulations provide evidences of the dynamical and thermal stabilities of cP-C24, respectively [64].

We next discuss the electronic properties of cP-C24. In Fig. 1(c), we show the bulk BZ and the projected (001) surface BZ, in which high-symmetry points are marked. As carbon exhibits the negligible SOC effect [55], a carbon allotrope can be treated as an ideal spinless system. Thus, in the main text, we only focus on the band structure without considering SOC and the discussion of SOC effect is presented in the SM [67]. The bulk electronic band structure along high-symmetry paths is shown in Fig. 2(a). The marked quadrangles of A, B, and C show three nonequivalent types of WPs, termed as WP₁, WP₂, and WP₃. Through carefully screening energy differences between the lowest conduction and the highest valence bands, we find that there are a total of 21 WPs over the whole BZ, including one WP₁ (CFWP) at the Γ point, twelve WP₂ (type-II Weyl) located at the $k_x = 0$, $k_y = 0$ and $k_z = 0$ planes, and eight WP₃ (type-I Weyl) along four

TABLE I. The calculated structural parameters, volumes per atom V_0 , total energies per atom E_{tot} and energy gaps E_g for different carbon allotropes, compared to reported data [48,59–64].

Allotrope	SG	Method	a (Å)	b (Å)	c (Å)	V_0 (Å ³ /atom)	E_{tot} (eV/atom)	E_g (eV)
cP-C24	$P4_132$	This work	5.960			8.84	−8.453	Semimetal
		GGA [64]	5.960			8.84		Metal
tP-C24	$P4/mmm$	GGA [59]	7.350		3.941	8.39	−8.052	2.68
oP-C24	$Pnna$	AM05 [48]	4.905	12.007	3.276	8.04	−8.723	Semimetal
ort-C24	$Cccm$	GGA [60]	12.890	4.004	4.991	10.76	−8.678	Semimetal
C24	$Cmm2$	GGA [61]	4.472	9.212	3.910	6.54	−8.613	2.94
Diamond	$Fd\bar{3}m$	GGA [62]	3.552			5.69	−9.092	5.36
		Expt. [62]	3.567			5.67		5.47
T-carbon	$Fd\bar{3}m$	GGA [63]	7.493			13.16	−7.919	2.25

diagonals [see their locations in the BZ in Fig. 1(c)]. To further explore the band topology depending on the crystal symmetry, we plot the enlarged drawings of energy dispersion around each of the WPs and mark the relevant irreducible representations (IRs) in Figs. 2(b)–2(d). The related symbols of IRs are listed in Tables SI–SIII in the SM [67]. The little group at the Γ point belongs to point group (PG) O , which possesses a two-dimensional (2D) IR Γ_3 corresponding to the twofold CFWP. According to compatible relations between group and subgroup (see Table SIV in the SM [67]), one can find that the 2D IR Γ_3 decomposes into two one-dimensional (1D) IRs Γ_1 and Γ_2 in PG C_2 along Γ -M direction. This allows the WP_2 to occur along the Γ -M path, which shows tilted linear dispersion, namely type-II WPs, see Fig. 2(c). Along the Γ -R direction, we consider two decomposed modes (see Table SIV and Fig. S2 in the SM [67]), (i) the 2D IR Γ_3 in PG O breaks into two 1D IRs Γ_2 and Γ_3 in PG C_3 , and (ii) the three-dimensional IR Γ_4 turns into three 1D IRs Γ_1 , Γ_2 , and Γ_3 . The crossing between the Γ_1 and Γ_3 bands results in the formation of WP_3 , showing a conventional Weyl fermion (type-I WP), as drawn in Fig. 2(d). The detailed information on the WPs is listed in Table II.

III. THE SYMMETRY ARGUMENTS AND TOPOLOGICAL SURFACE STATES

To confirm the twofold CFWP in cP-C24, we perform the symmetry arguments and construct the low-energy effective model at Γ . We first give the matrix representations of the symmetry operators. The chosen generators are the twofold screw symmetries $\{C_{2,001}|\frac{1}{2}0\frac{1}{2}\}$ and $\{C_{2,010}|\frac{1}{2}\frac{1}{2}\}$, the threefold screw symmetry $\{C_{3,111}^+|000\}$, the fourfold screw symmetry $\{C_{4,001}^+|\frac{1}{4}\frac{3}{4}\frac{1}{4}\}$, and time-reversal symmetry (\mathcal{T}). The basis state is chosen as $\varphi = \{|c_3 = e^{i\frac{2\pi}{3}}\rangle, |c_3 = e^{-i\frac{2\pi}{3}}\rangle\}$ with c_3 as the eigenvalue of $C_{3,111}^+$. Under this basis, the matrix

representations are given by

$$\begin{aligned}
 D(C_{2,001}) &= \sigma_0, \quad D(C_{2,010}) = D(C_{2,001}), \\
 D(C_{3,111}^+) &= \begin{bmatrix} e^{i\frac{2\pi}{3}} & 0 \\ 0 & e^{-i\frac{2\pi}{3}} \end{bmatrix}, \\
 D(C_{4,001}^+) &= \sigma_x, \quad D(\mathcal{T}) = \sigma_x \mathcal{K},
 \end{aligned} \tag{1}$$

where σ_0 is a 2×2 identity matrix, σ_i ($i = x, y, z$) are three Pauli matrices, and \mathcal{K} is the complex conjugate operator. The generators constrain the Hamiltonian as follows:

$$D(\mathcal{O})\mathcal{H}_\Gamma(\mathbf{k})D^{-1}(\mathcal{O}) = \mathcal{H}_\Gamma(\mathcal{O}\mathbf{k}). \tag{2}$$

Hence, the effective Hamiltonian up to the third order is derived as

$$\begin{aligned}
 \mathcal{H}_\Gamma(\mathbf{k}) &= D + Ek^2\sigma_0 + F(k_x^2 + k_y^2 - 2k_z^2)\sigma_x \\
 &\quad + F\sqrt{3}(k_y^2 - k_x^2)\sigma_y + Gk_xk_yk_z\sigma_z,
 \end{aligned} \tag{3}$$

where $k^2 = k_x^2 + k_y^2 + k_z^2$ and D , E , F , and G are real coefficients related to specific materials. This Hamiltonian (3) exhibits cubic dispersion along the [111] direction and quadratic band dispersion for any other directions. The Wannier charge centers (WCCs), by employing the Wilson-loop method [68], confirm that it is exactly the twofold CFWP with $C = +4$ (see Fig. S3 in the SM [67]).

We next examine the topological charges of different types of WPs in cP-C24 by the first-principles calculations. To proceed with this, we constructed a tight-binding (TB) Hamiltonian by projecting the Bloch states into maximally localized Wannier functions using the WANNIER90 package [69,70]. As shown in Fig. 3(a), the evolution of WCCs shows that the WP_1 possesses a topological charge of $C = +4$, which is consistent with our low energy effective Hamiltonian and further confirms the twofold CFWP. A large topological charge indicates lower energy dispersion near the critical point, which

TABLE II. The corresponding energies, positions, topological charges, types, and multiplicities of the inequivalent WPs in cP-C24.

Material	WP	$E-E_F$ (meV)	Coordinate (k_1, k_2, k_3)	Charge	Type	Multiplicity
cP-C24	WP_1	87.5	(0, 0, 0)	+4	CFWP	1
	WP_2	−29.2	(0.21, 0.21, 0)	−1	II	12
	WP_3	−60.3	(0.31, 0.31, 0.31)	+1	I	8

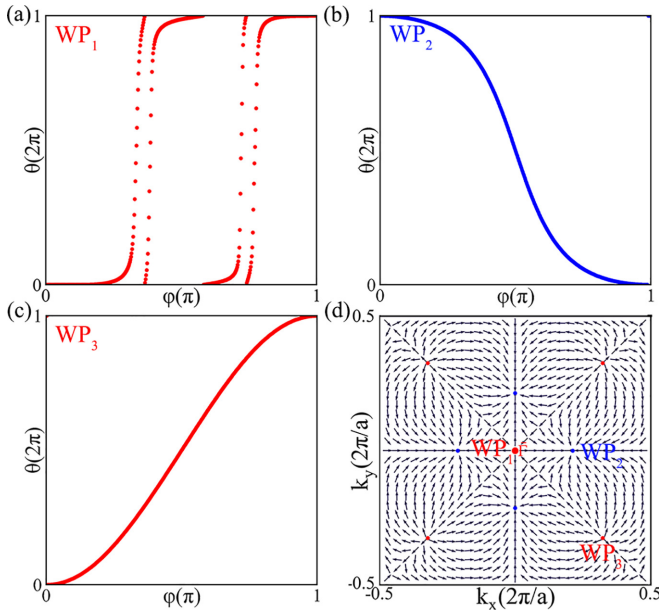


FIG. 3. (a)–(c) The evolutions of WCCs of the WPs for WP₁, WP₂, and WP₃, respectively, where $\varphi \in [0, \pi]$ is the polar angle and $\theta \in [0, 2\pi]$ is the azimuthal angle in spherical coordinate. The WPs are characterized by the topological charge of +4, -1, and +1, respectively. (d) The Berry curvature distribution on the (001) surface BZ. The WP₁ ($C = +4$) and WP₃ ($C = +1$) as the “source” flow into the “sink” generated by the WP₂ ($C = -1$).

provides an alternative avenue to investigate the electron-electron interactions in chiral fermions [71]. In Figs. 3(b) and 3(c), it shows that the WP₂ (WP₃) has a topological charge of $C = -1$ ($C = +1$). As drawn in Fig. 1(c), the red (blue) dots represent WPs with positive (negative) topological charge. Summing up all of the topological charges in the whole BZ, one can find it obeys the no-go theorem [72,73]. We also calculate the Berry curvature distribution as plotted in Fig. 3(d). It shows that the WP₁ ($C = +4$) and WP₃ ($C = +1$) as the “source” flow into the “sink” generated by the WP₂ ($C = -1$), which is in agreement with the signs of topological charges.

The symmetry-guaranteed twofold CFWP in cP-C24 should possess unique nontrivial quadruple helicoid surface states according to the bulk-boundary correspondence. To prove this, we compute the local density of states (LDOS) and Fermi arcs by employing the iterative Greens function method with the WannierTools package [74–76]. Here, the semi-infinite surface is constructed to obtain the LDOS on the (001) surface BZ. There are several topological surface states (TSSs) connecting different types of WPs, as shown in Fig. 4(a), while other TSSs are hidden in the projection of bulk states. To clearly show all the nontrivial surface states, three isoenergy contours are plotted at the energy levels of the three types of Weyl points. The isoenergy contour cut₁ at $E = 87.5$ meV is shown in Fig. 4(b). It shows the quadruple helicoid surface states: four surface sheets wind around the CFWP. We further compute the LDOS along a clockwise loop with $\bar{\Gamma}$ at its center, which shows that the four right-moving chiral edge modes appear inside the band gap [see the inset in 4(b)]. These are all the evidences of CFWP. Unlike spin- $\frac{3}{2}$

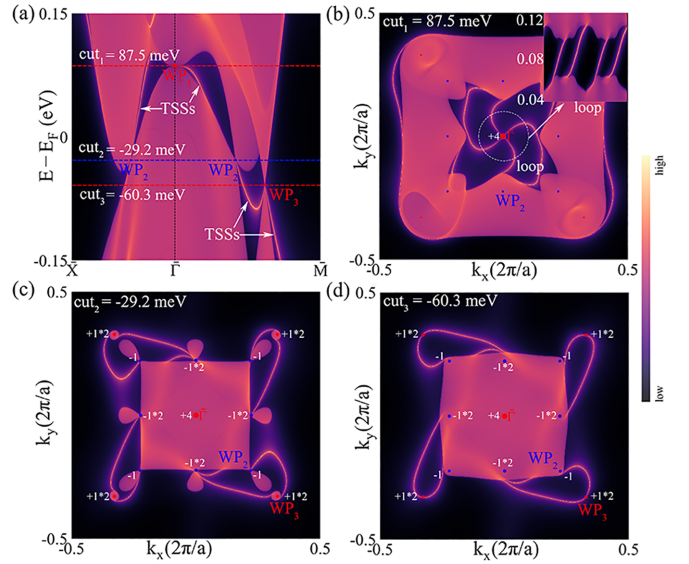


FIG. 4. (a) The LDOS along $\bar{X}-\bar{\Gamma}-\bar{M}$ on the (001) surface BZ. Topological surface states are marked by TSSs. The red and blue lines represent the different isoenergy contours at $E - E_F$. (b) The isoenergy contour cut₁ at $E = 87.5$ meV on the (001) surface BZ. The inset shows the four right-moving chiral edge modes connecting two regions. The two isoenergy contours (c) cut₂ ($E = -29.2$ meV) and (d) cut₃ ($E = -60.3$ meV) on the (001) surface BZ and the positions of the WPs associated with the topological charges.

systems, in which the TSSs depend on the strength of SOC, the quadruple helicoid surface states in twofold CFWP are distinct and well-separated, making them easier to be detected by experiments. The other two isoenergy contours cut₂ ($E = -29.2$ meV) and cut₃ ($E = -60.3$ meV) are also illustrated in Figs. 4(c) and 4(d), respectively. The positions of the WPs associated with topological charges are marked. There are two TSSs coming out from the projections of WP₂ since this surface double Weyl point projected from two WPs with negative topological charge. Similarly, the projection of WP₃ on the (001) surface also exhibits two TSSs due to the projected double Weyl point. The nontrivial Fermi arcs are highly visible and long, indicating their potential for experimental observation. Since the CFWP is protected by crystalline symmetry, it will evolve into different types of WPs under symmetry broken. Here, we prove that the number and topological charge of the WPs and the TSSs can be tuned by applying 1% uniaxial strain along the [001] and [111] directions, respectively (see Figs. S8 and S9 in the SM [67]).

IV. SUMMARY

In summary, based on the symmetry arguments and first-principles calculations, we identify a carbon allotrope cP-C24 as an ideal material to hold twofold CFWP. The CFWP, located at the $\bar{\Gamma}$ point, can generate visible quadruple helicoid surface states on the (001) surface BZ due to the bulk-boundary correspondence. Because the twofold CFWP is independent of SOC, the induced quadruple helicoid surface states are well separated from each other compared to that in spin- $\frac{3}{2}$ fermions, making them easier to be detected by

experiments. Besides, due to the large topological charge, the near-flat band around the CFWP provides a platform to study the electron-electron interactions in chiral fermions. A large topological charge can also give rise to a significant quantized CPGE, making it a promising avenue for potential applications. Our findings not only identify an ideal candidate to design CFWP but also provide a platform to explore novel properties in carbon allotropes.

ACKNOWLEDGMENTS

This work was supported by the National Natural Science Foundation of China (NSFC, Grants No. 12174040, No. 12204074, No. 12222402, No. 11974062, and No. 12147102), the China National Postdoctoral Program for Innovative Talent (Grant No. BX20220367), and Chongqing Natural Science Foundation (Grant No. cstc2020jcyj-msxmX0118).

-
- [1] B. Bradlyn, J. Cano, Z. Wang, M. G. Vergniory, C. Felser, R. J. Cava, and B. A. Bernevig, *Science* **353**, aaf5037 (2016).
- [2] B. J. Wieder, Y. Kim, A. M. Rappe, and C. L. Kane, *Phys. Rev. Lett.* **116**, 186402 (2016).
- [3] S.-M. Huang, S.-Y. Xu, I. Belopolski, C.-C. Lee, G. Chang, T.-R. Chang, B. Wang, N. Alidoust, G. Bian, M. Neupane, D. Sanchez, H. Zheng, H.-T. Jeng, A. Bansil, T. Neupert, H. Lin, and M. Z. Hasan, *Proc. Natl. Acad. Sci. USA* **113**, 1180 (2016).
- [4] A. Bouhon and A. M. Black-Schaffer, *Phys. Rev. B* **95**, 241101(R) (2017).
- [5] Z. Song and X. Dai, *Phys. Rev. X* **9**, 021053 (2019).
- [6] J. Xiang, S. Hu, Z. Song, M. Lv, J. Zhang, L. Zhao, W. Li, Z. Chen, S. Zhang, J.-T. Wang, Y.-f. Yang, X. Dai, F. Steglich, G. Chen, and P. Sun, *Phys. Rev. X* **9**, 031036 (2019).
- [7] X. Huang, L. Zhao, Y. Long, P. Wang, D. Chen, Z. Yang, H. Liang, M. Xue, H. Weng, Z. Fang, X. Dai, and G. Chen, *Phys. Rev. X* **5**, 031023 (2015).
- [8] D. T. Son and B. Z. Spivak, *Phys. Rev. B* **88**, 104412 (2013).
- [9] A. A. Zyuzin and A. A. Burkov, *Phys. Rev. B* **86**, 115133 (2012).
- [10] J. Xiong, S. K. Kushwaha, T. Liang, J. W. Krizan, M. Hirschberger, W. Wang, R. J. Cava, and N. P. Ong, *Science* **350**, 413 (2015).
- [11] J. Cano, B. Bradlyn, Z. Wang, M. Hirschberger, N. P. Ong, and B. A. Bernevig, *Phys. Rev. B* **95**, 161306(R) (2017).
- [12] H. Jia, R. Zhang, W. Gao, Q. Guo, B. Yang, J. Hu, Y. Bi, Y. Xiang, C. Liu, and S. Zhang, *Science* **363**, 148 (2019).
- [13] C. Fang, M. J. Gilbert, X. Dai, and B. A. Bernevig, *Phys. Rev. Lett.* **108**, 266802 (2012).
- [14] S. S. Tsirkin, I. Souza, and D. Vanderbilt, *Phys. Rev. B* **96**, 045102 (2017).
- [15] Y. J. Jin, Y. Xu, Z. J. Chen, and H. Xu, *Phys. Rev. B* **105**, 035141 (2022).
- [16] W. Wu, Z.-M. Yu, X. Zhou, Y. X. Zhao, and S. A. Yang, *Phys. Rev. B* **101**, 205134 (2020).
- [17] N. B. M. Schroter, S. Stolz, K. Manna, F. de Juan, M. G. Vergniory, J. A. Krieger, D. Pei, T. Schmitt, P. Dudin, T. K. Kim, C. Cacho, B. Bradlyn, H. Borrmann, M. Schmidt, R. Widmer, V. N. Strocov, and C. Felser, *Science* **369**, 179 (2020).
- [18] E. J. König, H.-Y. Xie, D. A. Pesin, and A. Levchenko, *Phys. Rev. B* **96**, 075123 (2017).
- [19] F. de Juan, A. G. Grushin, T. Morimoto, and J. E. Moore, *Nat. Commun.* **8**, 15995 (2017).
- [20] F. Flicker, F. de Juan, B. Bradlyn, T. Morimoto, M. G. Vergniory, and A. G. Grushin, *Phys. Rev. B* **98**, 155145 (2018).
- [21] S.-Y. Xu, I. Belopolski, N. Alidoust, M. Neupane, G. Bian, C. Zhang, R. Sankar, G. Chang, Z. Yuan, C.-C. Lee, S.-M. Huang, H. Zheng, J. Ma, D. S. Sanchez, B. Wang, A. Bansil, F. Chou, P. P. Shibayev, H. Lin, S. Jia, and et al., *Science* **349**, 613 (2015).
- [22] B. Q. Lv, H. M. Weng, B. B. Fu, X. P. Wang, H. Miao, J. Ma, P. Richard, X. C. Huang, L. X. Zhao, G. F. Chen, Z. Fang, X. Dai, T. Qian, and H. Ding, *Phys. Rev. X* **5**, 031013 (2015).
- [23] L. Lu, Z. Wang, D. Ye, L. Ran, L. Fu, J. D. Joannopoulos, and M. Soljacic, *Science* **349**, 622 (2015).
- [24] P. Tang, Q. Zhou, and S.-C. Zhang, *Phys. Rev. Lett.* **119**, 206402 (2017).
- [25] G. Chang, S.-Y. Xu, B. J. Wieder, D. S. Sanchez, S.-M. Huang, I. Belopolski, T.-R. Chang, S. Zhang, A. Bansil, H. Lin, and M. Z. Hasan, *Phys. Rev. Lett.* **119**, 206401 (2017).
- [26] D. Takane, Z. Wang, S. Souma, K. Nakayama, T. Nakamura, H. Oinuma, Y. Nakata, H. Iwasawa, C. Cacho, T. Kim, K. Horiba, H. Kumigashira, T. Takahashi, Y. Ando, and T. Sato, *Phys. Rev. Lett.* **122**, 076402 (2019).
- [27] Z. Rao, H. Li, T. Zhang, S. Tian, C. Li, B. Fu, C. Tang, L. Wang, Z. Li, W. Fan, J. Li, Y. Huang, Z. Liu, Y. Long, C. Fang, H. Weng, Y. Shi, H. Lei, Y. Sun, T. Qian, and et al., *Nature (London)* **567**, 496 (2019).
- [28] S.-K. Jian and H. Yao, *Phys. Rev. B* **92**, 045121 (2015).
- [29] S.-K. Jian and H. Yao, *Phys. Rev. B* **96**, 155112 (2017).
- [30] E.-G. Moon, C. Xu, Y. B. Kim, and L. Balents, *Phys. Rev. Lett.* **111**, 206401 (2013).
- [31] I. F. Herbut and L. Janssen, *Phys. Rev. Lett.* **113**, 106401 (2014).
- [32] T. Zhang, R. Takahashi, C. Fang, and S. Murakami, *Phys. Rev. B* **102**, 125148 (2020).
- [33] Q.-B. Liu, Z. Wang, and H.-H. Fu, *Phys. Rev. B* **103**, L161303 (2021).
- [34] C. Cui, X.-P. Li, D.-S. Ma, Z.-M. Yu, and Y. Yao, *Phys. Rev. B* **104**, 075115 (2021).
- [35] Z.-M. Yu, Z. Zhang, G.-B. Liu, W. Wu, X.-P. Li, R.-W. Zhang, S. A. Yang, and Y. Yao, *Sci. Bull.* **67**, 375 (2022).
- [36] X. Wang, F. Zhou, Z. Zhang, W. Wu, Z.-M. Yu, and S. A. Yang, *Phys. Rev. B* **106**, 195129 (2022).
- [37] Z.-Q. Wang, Q.-B. Liu, X.-F. Yang, and H.-H. Fu, *Phys. Rev. B* **106**, L161302 (2022).
- [38] Q. Chen, F. Chen, Y. Pan, C. Cui, Q. Yan, L. Zhang, Z. Gao, S. A. Yang, Z.-M. Yu, H. Chen, B. Zhang, and Y. Yang, *Nat. Commun.* **13**, 7359 (2022).
- [39] L. Luo, W. Deng, Y. Yang, M. Yan, J. Lu, X. Huang, and Z. Liu, *Phys. Rev. B* **106**, 134108 (2022).
- [40] J. D. Koralek, C. P. Weber, J. Orenstein, B. A. Bernevig, S.-C. Zhang, S. Mack, and D. D. Awschalom, *Nature (London)* **458**, 610 (2009).
- [41] S. Wu, Z. Yang, A.-M. Guo, and F. Ouyang, *Phys. E* **126**, 114457 (2021).
- [42] C. Zhang, X.-Y. Ding, L.-Y. Gan, Y. Cao, B.-S. Li, X. Wu, and R. Wang, *Phys. Rev. B* **101**, 235119 (2020).

- [43] W. Wu, Y. Xie, and Y. Chen, *Phys. Rev. Mater.* **5**, 104201 (2021).
- [44] T. Deng, B. Zheng, F. Zhan, J. Fan, X. Wu, and R. Wang, *Phys. Rev. B* **102**, 201105(R) (2020).
- [45] H. Weng, Y. Liang, Q. Xu, R. Yu, Z. Fang, X. Dai, and Y. Kawazoe, *Phys. Rev. B* **92**, 045108 (2015).
- [46] J.-T. Wang, H. Weng, S. Nie, Z. Fang, Y. Kawazoe, and C. Chen, *Phys. Rev. Lett.* **116**, 195501 (2016).
- [47] Y. Cheng, X. Feng, X. Cao, B. Wen, Q. Wang, Y. Kawazoe, and P. Jena, *Small* **13**, 1602894 (2017).
- [48] K. Bu, Y. Qian, J.-T. Wang, and H. Weng, *Phys. Rev. B* **103**, L081108 (2021).
- [49] J.-T. Wang, S. Nie, H. Weng, Y. Kawazoe, and C. Chen, *Phys. Rev. Lett.* **120**, 026402 (2018).
- [50] Y. Chen, Y. Xie, S. A. Yang, H. Pan, F. Zhang, M. L. Cohen, and S. Zhang, *Nano Lett.* **15**, 6974 (2015).
- [51] C. Zhong, Y. Chen, Y. Xie, S. A. Yang, M. L. Cohen, and S. B. Zhang, *Nanoscale* **8**, 7232 (2016).
- [52] Y. Qie, J. Liu, S. Wang, Q. Sun, and P. Jena, *J. Mater. Chem. A* **7**, 5733 (2019).
- [53] J. Zhang, R. Wang, X. Zhu, A. Pan, C. Han, X. Li, D. Zhao, C. Ma, W. Wang, H. Su, and C. Niu, *Nat. Commun.* **8**, 683 (2017).
- [54] X.-W. Yi, Z. Zhang, Z.-W. Liao, X.-J. Dong, J.-Y. You, and G. Su, *Nano Today* **42**, 101346 (2022).
- [55] Y. Yao, F. Ye, X.-L. Qi, S.-C. Zhang, and Z. Fang, *Phys. Rev. B* **75**, 041401(R) (2007).
- [56] A. Hirsch, *Nat. Mater.* **9**, 868 (2010).
- [57] J.-W. J. Run-Sen Zhang, *Front. Phys.* **14**, 13401 (2019).
- [58] X. Shi, C. He, C. J. Pickard, C. Tang, and J. Zhong, *Phys. Rev. B* **97**, 014104 (2018).
- [59] Q. Fan, H. Wang, Y. Song, W. Zhang, and S. Yun, *Comput. Mater. Sci.* **178**, 109634 (2020).
- [60] Z.-L. Lv, H.-L. Cui, and C. Cheng, *Phys. Chem. Chem. Phys.* **24**, 23497 (2022).
- [61] M. Xing, C. Qian, and X. Li, *J. Solid State Chem.* **309**, 122971 (2022).
- [62] F. Occelli, P. Loubeyre, and R. LeToullec, *Nat. Mater.* **2**, 151 (2003).
- [63] X.-L. Sheng, Q.-B. Yan, F. Ye, Q.-R. Zheng, and G. Su, *Phys. Rev. Lett.* **106**, 155703 (2011).
- [64] Z. Wang, X. Zhu, and M. Wang, *Solid State Sci.* **105**, 106247 (2020).
- [65] P. Hohenberg and W. Kohn, *Phys. Rev.* **136**, B864 (1964).
- [66] W. Kohn and L. Sham, *Phys. Rev.* **140**, A1133 (1965).
- [67] See Supplemental Material at <http://link.aps.org/supplemental/10.1103/PhysRevB.108.075130> for details of the calculations, the stability of cP-C24, character table of the point group, band structure with/without SOC, the effective Hamiltonian fitting band structures, and relevant WCCs, which includes Refs. [64–66,68–70,74–81].
- [68] R. Yu, X. L. Qi, A. Bernevig, Z. Fang, and X. Dai, *Phys. Rev. B* **84**, 075119 (2011).
- [69] N. Marzari and D. Vanderbilt, *Phys. Rev. B* **56**, 12847 (1997).
- [70] A. A. Mostofi, J. R. Yates, Y.-S. Lee, I. Souza, D. Vanderbilt, and N. Marzari, *Comput. Phys. Commun.* **178**, 685 (2008).
- [71] J. E. Drut and T. A. Lähde, *Phys. Rev. B* **79**, 165425 (2009).
- [72] H. Nielsen and M. Ninomiya, *Nucl. Phys. B* **185**, 20 (1981).
- [73] H. Nielsen and M. Ninomiya, *Nucl. Phys. B* **193**, 173 (1981).
- [74] M. P. L. Sancho, J. M. L. Sancho, and J. Rubio, *J. Phys. F* **14**, 1205 (1984).
- [75] M. P. L. Sancho, J. M. L. Sancho, J. M. L. Sancho, and J. Rubio, *J. Phys. F* **15**, 851 (1985).
- [76] Q. Wu, S. Zhang, H.-F. Song, M. Troyer, and A. A. Soluyanov, *Comput. Phys. Commun.* **224**, 405 (2018).
- [77] G. Kresse and J. Furthmüller, *Comput. Mater. Sci.* **6**, 15 (1996).
- [78] G. Kresse and J. Furthmüller, *Phys. Rev. B* **54**, 11169 (1996).
- [79] J. P. Perdew, K. Burke, and M. Ernzerhof, *Phys. Rev. Lett.* **77**, 3865 (1996).
- [80] P. E. Blöchl, *Phys. Rev. B* **50**, 17953 (1994).
- [81] H. J. Monkhorst and J. D. Pack, *Phys. Rev. B* **13**, 5188 (1976).